RSC Advances

ROYAL SOCIETY OF CHEMISTRY

www.rsc.org/advances

RSC ADV

ARTICLE

Hybrid SnO_2-Co_3O_4 nanocubes prepared via $CoSn(OH)_6$ intermediate through sonochemical route for Energy Storage Applications

Cite this: DOI: 10.1039/x0xx00000x

Balasubramaniam Gnana Sundara Raj[a], Jerry J Wu[b], Abdullah M. Asiri[c], Sambandam Anandan[a,*]

Received 00th January 2012,
Accepted 00th January 2012

DOI: 10.1039/x0xx00000x

www.rsc.org/

Cubic like nanostructured SnO_2-Co_3O_4 hybrid was sonochemically synthesized via formation of $CoSn(OH)_6$ nanocubes as intermediate at room temperature in the presence of stannous and cobalt precursors, without the assistance of any surfactant or template. The obtained hybrid was maintaining the original frame structure of $CoSn(OH)_6$ nanocubes. The above samples were characterized by Thermal gravimetric analysis (TGA), X-ray powder diffraction (XRD), Fourier transform infrared spectroscopy (FT-IR), Scanning electron microscope (SEM), Transmission electron microscopy (TEM) and Energy-dispersive X-ray spectroscopy (EDX) analysis. The electrochemical performance of the hybrid SnO_2-Co_3O_4 nanocubes was investigated as supercapacitor electrode materials through cyclic voltammetry (CV), galvanostatic charge–discharge and electrochemical impedance spectroscopy (EIS) studies. The cubic like nanostructured hybrid SnO_2-Co_3O_4 exhibit enhanced supercapacitor performances. The hybrid SnO_2-Co_3O_4 nanocube delivered a maximum specific capacitance of 484 F g^{-1}, which was more than four-fold higher than bare SnO_2 (101 F g^{-1}) and intermediate $CoSn(OH)_6$ nanocubes at the same current density of 0.5 mA cm^{-2} in the potential range between 0 to +1 V. The enhancement of the overall electrochemical behaviour of the electrode material can be attributed to the synergetic effect between nanostructured SnO_2 and Co_3O_4. About 77% of its initial capacitance was retained after 1000 cycles demonstrates its high electrochemical stability and capacitance retention also. The obtained results confirmed that this material is promising candidate for supercapacitor applications.

1. Introduction

Electrochemical capacitors (ECs) or supercapacitors has been much attention among various electrical energy storage devices due to their amazing properties like high power density, fast charge-discharge rate and long operating lifetimes.[1] Currently, ECs are greatly applied in hybrid electric vehicles, back-up power devices, pulse power etc.[2,3] Generally the supercapacitors can be classified into two categories based on the charge storage mechanism: (i) electrochemical double-layer capacitors (EDLCs), which are based on electrostatic charge diffusion and accumulation at the electrode/electrolyte interface[4], (ii) pseudocapacitors, which are based on reversible faradic redox reactions at the electrode/electrolyte interface.[5] In recent years, a significant amount of effort has been assigned to improve the electrochemical performance of electrode materials in order to develop better supercapacitors with both high power and energy densities.[6] To date, the electrode materials used for supercapacitors are carbon materials (activated carbons[7], carbon fabrics[8], carbon nanotubes[9], etc.), transition metal oxides (RuO_2[10], MnO_2[11], Co_3O_4[12], NiO[13], SnO_2[14], etc.) and conducting polymers (polyaniline[15], polypyrrole[16], polythiophene[17], etc.). Carbon materials with high surface area have been most widely used in supercapacitors but the main drawback is low average specific capacitance value of this materials.[18] Nowadays, pseudocapacitive materials are great concerns by researchers with their excellent electrochemical properties such as conducting polymers and metal oxides.[17, 19] The specific capacitances of the pseudocapacitive materials have higher capacitive nature than carbonaceous materials depending upon charge storage mechanism.[20] Transition metal oxides were used as electrode materials for supercapacitors due to their high redox pseudo capacitance, chemical stability, and variable valence states.[21] RuO_2 have been widely used as electrode materials because of its high-energy storage capabilities with large specific capacitance and good reversibility. However, it has limited practical applications owing to the lack of abundance, high cost and toxicity of this oxide.[22] Upon compared to RuO_2, the current research focus on other metal oxides such as MnO_2[11], Co_3O_4[12], NiO[13] and SnO_2[14]. Among these oxides, SnO_2 being cost-effective and environmentally benign, are a kind of promising materials that have wide applications in supercapacitors[14], lithium ion batteries[23], dye-based solar cells[24], catalysts[25], gas sensors[26] and so on.

Recently, composites of metal oxides (Co_3O_4–NiO[27], MnO_2 –NiO[28], etc.) and metal oxide/hydroxide composite ($Ni(OH)_2$ –MnO_2 [29], Co_3O_4 – $Ni(OH)_2$[30], etc.) has been used to develop supercapacitors. Based on available literature reported that multiple oxide materials exhibit superior capacitive performance compared to single transition metal oxides. It has been demonstrated that various metal oxides such as Fe_3O_4[31], RuO_2[22], V_2O_5[32] and MnO_2[33] oxides added to bare SnO_2, shows enhanced electrical conductivity and specific capacitance compared that of bare SnO_2. Cobalt oxide (Co_3O_4) has been studied as a promising potential candidate for supercapacitor electrode materials because of its environmental friendliness, low cost and pseudocapacitance allows larger charge storage.[34] However, the electrochemical capacitive properties of cobalt oxide coupled with SnO_2 have received relatively little attention.[35, 36] To prepare homogeneous dispersions of multiple oxides depending on the synthetic route[36],

various synthetic methods such as hydrothermal method[35], solvothermal[37], co-precipitation[38], etc are used for the preparation of tin oxide composite. Among these synthetic approaches, sonochemical method was possible method towards synthesizing multiple oxides through the principle of acoustic cavitation; the formation, growth, and implosive collapse of bubbles in a liquid. Bubble collapse stimulated by cavitation produces intense local heating and high pressures.[11]

In this work, cubic like nanostructured SnO_2-Co_3O_4 coupled hybrid was sonochemically synthesized via formation of $CoSn(OH)_6$ nanocubes as intermediate and investigate their strength towards supercapacitor applications. Remarkably, these cubic like nanostructured SnO_2-Co_3O_4 coupled hybrid exhibit high specific capacitance and attractive rate capability compared to $CoSn(OH)_6$ nanocubes intermediate, bare SnO_2 and could be a promising candidate for electrode material in supercapacitor applications.

2. Experimental

2.1. Materials

All reagents are analytically pure and used without further purification. Stannic chloride ($SnCl_4.5H_2O$, 98%) and Cobalt chloride ($CoCl_2.6H_2O$, 97%) were purchased from Sigma-Aldrich. Sodium hydroxide pellets (NaOH, 98 wt %) was purchased from SRL Pvt. Ltd, India. Vulcan XC-72 and poly-vinylidene fluoride (PVdF) was purchased from Fluka. N-methyl-2-pyrrolidone (NMP) was purchased from Merck. All solutions for the experiments were prepared with doubly distilled (DD) water.

2.2 Sonochemical preparation of SnO_2-Co_3O_4 coupled hybrid

A horn type 20 kHz Sonics sonifier (100 W/cm^2) with a tip diameter of 13 mm was used for sonication. In a typical sonochemical synthesis, 0.642 g of $CoCl_2.6H_2O$ and 1.893g of $SnCl_4.5H_2O$ according to the mole ratio (1:2) were dissolved in 60 ml of DD water to form pink colour solution under continuous magnetic stirring. Then, 1.8 g of NaOH dissolved in 30 ml of DD water was added to the above solution slowly. After addition, the solution was stirred at room temperature for 10 min, and then irradiated with ultrasound for 30 min. After 30 min, the pink colour precipitate ($CoSn(OH)_6$) was obtained. Then the precipitate was centrifuged, washed with DD water several times and then with ethanol. It was dried in air at room temperature. Then the product was calcined at 500 °C for 2 h under air at a heating rate of 5 °C min^{-1} to generate the black colour SnO_2-Co_3O_4 coupled hybrid. By following the same procedure, bare SnO_2 and pristine Co_3O_4 was prepared for comparative studies.

2.3 Characterization of materials

In order to confirm the crystal structure and phase purity of the product, powder X-ray diffraction patterns were recorded on a Philips XPertPro X-ray diffractometer with Cu Kα (λ = 0.15418 nm) radiation. FT-IR spectra were obtained with a Thermo Scientific Nicolet iS5 FT-IR spectrometer using a KBr pellet. The structural and morphology properties of the sample was studied using a JEOL 7401F (Scanning electron microscope) and JEOL JEM 2010 (High resolution transmission electron microscopy) model.

2.4 Electrochemical measurements

A supercapacitor electrode was prepared using a high-purity stainless steel (SS) plate as a current collector. The plate was polished with successive grades of emery paper, cleaned with soap solution, washed with DD water, rinsed with acetone, dried and weighed. The working electrode is made up of black color SnO_2-Co_3O_4 coupled hybrid or pink colour ($CoSn(OH)_6$) precipitate (75 wt.%) as an active material, Vulcan XC-72 carbon (20 wt.%) as a conductive agent, PVdF (5 wt.%) as a binder were ground in a mortar, and a few drops of NMP was added to form slurry. It was coated onto the pretreated SS plate (coating electrode area is 1.0 cm^2) and dried at 100 °C in vacuum for 12 h. Cyclic voltammetry (CV), galvanostatic charge–discharge and electrochemical impedance spectroscopy (EIS) techniques were carried at room temperature by using a potentiostat/galvanostat (AUTOLAB 302 N module) testing system.

The supercapacitance studies were carried out in a standard three-electrode system containing the black colour SnO_2-Co_3O_4 coupled hybrid coated stainless steel plate as a working electrode, Pt foil as a counter electrode and Ag/AgCl as a reference electrode. The electrolyte used was aqueous solution of 1M Na_2SO_4. The performance of supercapacitor studies were evaluated by cyclic voltammetry (CV) and galvanostatic charge–discharge techniques within the potential range between 0 to 1 V at different scan rates (5, 10, 20, 40, 80 and 160 mV s^{-1}) and different current densities (0.5-15 mA cm^{-2}) respectively. Electrochemical impedance spectroscopy measurements were performed under open circuit voltage in an alternating current frequency range of 0.1–1,00,000 Hz with an excitation signal of 10 mV. As a comparison, the electrochemical performance of $CoSn(OH)_6$ and bare SnO_2 was also investigated under the same conditions.

3. Results and discussion

As detailed in the experimental section, upon sonication of $CoCl_2.6H_2O$ and $SnCl_4.5H_2O$, a pink color intermediate product $CoSn(OH)_6$ was obtained and it is identified by XRD analysis (Fig. 1(a)). All the diffraction peaks at 2θ values of 19.9° (111), 23.0° (200), 32.7° (220), 36.9° (310), 38.3° (311), 40.4° (222), 47.1° (400), 51.5° (331), 52.9° (420), 58.2° (422), 61.9° (511), 68.3° (440), 71.9° (531), 73.1° (442), 77.7° (620) are perfectly indexed and matches well with the corresponding cubic $CoSn(OH)_6$ phase (JCPDS card no. 13–356). No signals from any other impurities indicates synthesized sample was pure and consist of only cubic $CoSn(OH)_6$ phase. The FT-IR spectra of the $CoSn(OH)_6$ shows O-H stretching at 3200 cm^{-1} (Fig. 1(b)) agrees well with the data available from the literature, where the hydroxyl ion is among the main components of the structural units of minerals.[39] The sharp peak observed at 1182 cm^{-1} may be due to Sn-OH bending vibration, peak at 784 cm^{-1} may be attributed to water-water hydrogen bonding[39] and peak at 544 cm^{-1} may be due to Co-O stretching vibration. Fig. 1(c) shows the TGA curve of $CoSn(OH)_6$ intermediate. No weight loss was observed from the TG curve at temperature above 300 °C indicates that the phase transition may takes place from the amorphous to the crystalline state.[40] Fig. 1(d) shows the FESEM images of $CoSn(OH)_6$ and it can be seen that the comprised of plenty of nanocubes with

smooth surfaces and the sizes of the nanocubes range from ~ 70 to 300 nm.

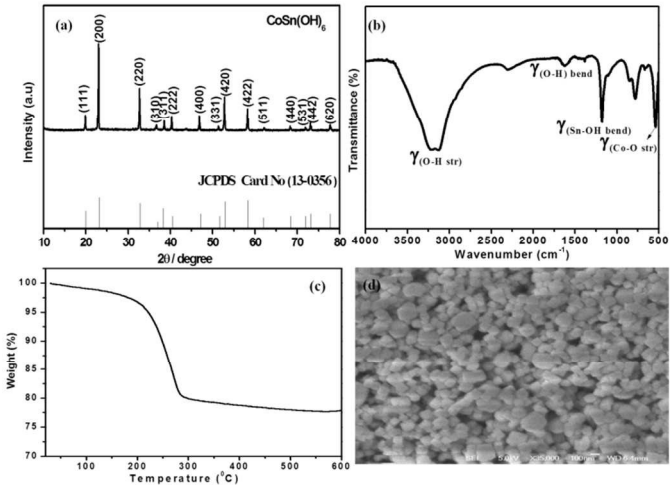

Fig. 1 (a) XRD pattern (b) FT-IR spectrum of (c) TGA curve (d) FESEM image of intermediate $CoSn(OH)_6$.

However upon calcination at 500°C, $CoSn(OH)_6$ yields the black colour SnO_2-Co_3O_4 coupled hybrid which is identified by the typical powder XRD pattern (Fig. 2). Upon viewing the XRD pattern, found that the diffraction peaks of $CoSn(OH)_6$ get disappeared and new diffraction peaks at 2θ values of 26.5° (110), 33.7° (101), 42.4° (210), 51.7° (211), 54.7° (220), 61.9° (221), 64.7° (301), 71.6° (202), 77.6° (321), 83.9° (410) are perfectly indexed and matches well with the corresponding tetragonal SnO_2 nanoparticles (JCPDS No. 77-0452). Beside this, the diffraction peaks appeared at 2θ values of 18.9° (111), 31.1° (220), 36.6° (311), 38.0° (222), 44.4° (400), 59.3° (511) are perfectly indexed and matches well with the corresponding cubic Co_3O_4 nanoparticles (JCPDS No. 78-1969). The absence of any other peak indicates that the SnO_2-Co_3O_4 coupled hybrid phase formation is made of both tetragonal SnO_2 and cubic Co_3O_4 phase only. Absence of $CoSnO_3$ diffraction peaks also illustrates that the formation of SnO_2-Co_3O_4 coupled hybrid only.

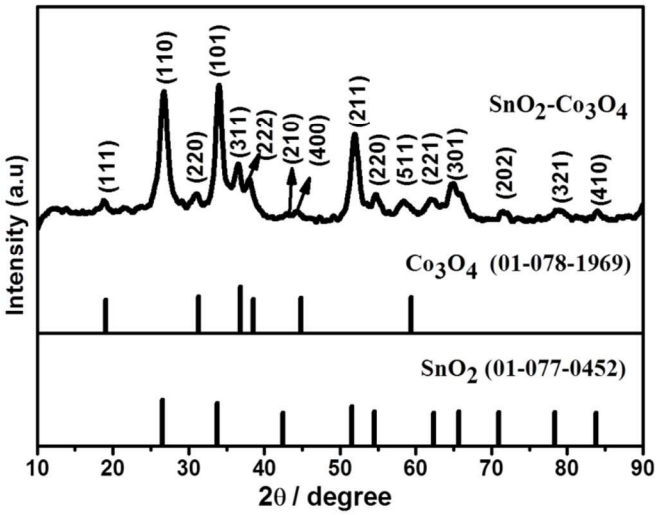

Fig. 2 The XRD pattern of SnO_2-Co_3O_4 coupled hybrid

Fig. 3 shows the FT-IR spectra of the SnO_2-Co_3O_4 coupled hybrid, the broad absorption band at 573 cm^{-1} due to Co-O stretching vibration mode. The sharp Sn-OH intermediate peak at 1182 cm^{-1} was disappeared and a new peak noticed at 653 cm^{-1} can be assigned as Sn-O stretching vibration[41], which clearly demonstrates that the presence of multiple oxide composite. The strong and weak absorption bands at 3425 cm^{-1} and 1632 cm^{-1} may be assigned due to O-H stretching and bending vibrations and these peaks represents the adsorption of moisture present on the surface of the sample.

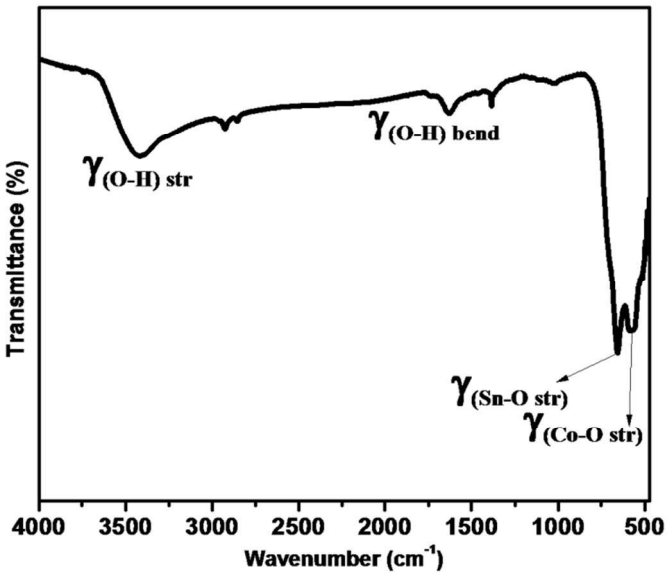

Fig. 3 FT-IR spectrum of SnO_2-Co_3O_4 coupled hybrid

The morphologies of the SnO_2-Co_3O_4 coupled hybrid have been investigated by using FE-SEM and HR-TEM analysis. FE-SEM image (Fig. 4 (a & b)) of SnO_2-Co_3O_4 coupled hybrid also looks like nanocube morphology similar to the structure of $CoSn(OH)_6$ but the sizes of nanocubes found decreased from 20-100 nm due to heat treatment. For comparison FESEM images of (a) bare SnO_2 and (b) pristine Co_3O_4 as shown in Fig. S1

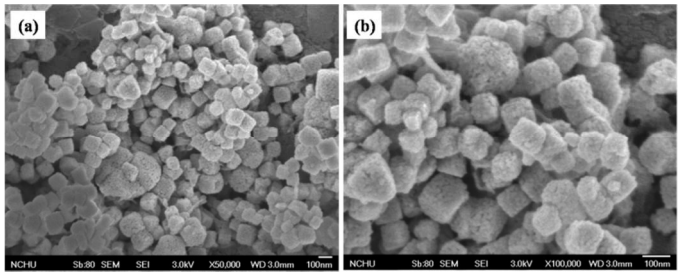

Fig. 4 FESEM images of SnO_2-Co_3O_4 coupled hybrid (a and b) at different magnifications, respectively.

HR-TEM images (Fig. 5 (a & b)) of SnO_2-Co_3O_4 coupled hybrid also illustrate the cubical shapes as confirmed by the FE-SEM observations. Fig. 5(c) describes a typical HR-TEM image of the coupled hybrid in which the lattice fringes are clearly seen and matches well with d-spacing 0.336 nm and 0.243 nm, corresponding to the (110) and (311) planes of tetragonal SnO_2 (JCPDS No. 77-0452) and cubic Co_3O_4 (JCPDS No. 78-1969) form respectively. The selected area electron diffraction (SAED) pattern (Fig. 5(d)) shows the crystalline nature of SnO_2-Co_3O_4 coupled hybrid and in addition the observed four diffraction rings can be assigned as (110), (331), (220), and (511) planes of tetragonal SnO_2 and cubic Co_3O_4 nanoparticles. The energy-dispersive X-ray spectroscopy (EDX)

shows the presence of Sn, Co, O composition of elements only in the coupled hybrid (Fig. 5(e)).

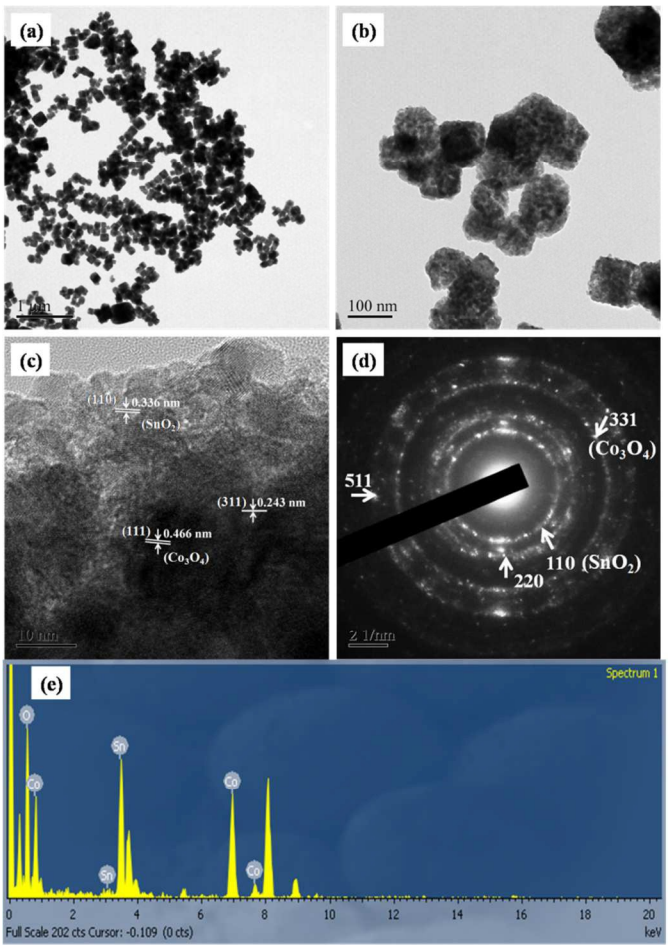

Fig. 5 HR-TEM images of SnO_2-Co_3O_4 coupled hybrid (a, b and c), corresponding SAED pattern (d) and EDX (e) spectrum.

The electrochemical properties of SnO_2-Co_3O_4 coupled hybrid as electrode material for supercapacitor were evaluated by cyclic voltammetry (CV), galvanostatic charge-discharge and EIS. As a comparison, the electrochemical performance of bare SnO_2 intermediate $CoSn(OH)_6$ and pristine Co_3O_4 was also investigated under the same conditions. Fig. 6 (a) shows the CV curves of bare SnO_2, intermediate $CoSn(OH)_6$, pristine Co_3O_4 and SnO_2-Co_3O_4 coupled hybrid electrode measured at a scan rate of 40 mV s^{-1} between 0 to +1 V *vs.* Ag/AgCl in 1 M Na_2SO_4 aqueous electrolyte. All the curves are rectangular in shape and in addition no redox transitions in the potential region illustrates the ideal capacitive behavior of the prepared electrodes. It is known that the specific capacitance is proportional to the integrated area of CVs.[42] Among the CV curves, the integrated area of SnO_2-Co_3O_4 coupled hybrid is the biggest, which means that this coupled hybrid has the largest capacitance in comparison with bare SnO_2, intermediate $CoSn(OH)_6$ and pristine Co_3O_4 sample. The capacitance of the SnO_2-Co_3O_4 coupled hybrid was enhanced due to the synergistic effect between the two different metal oxides which is responsible for the improved electrical conductivity, provide free diffusion pathways for the fast ion transport and facile ion accessibility to storage sites.[19] Fig. 6 (b) shows the CV curves of SnO_2-Co_3O_4 coupled hybrid electrode at different scan rates of 5-160 mV s^{-1}. All the CV curves are rectangular in shape and exhibit mirror image characteristics which clearly indicate that the electrochemical reactions are reversible and as well as an ideal electrochemical capacitive behavior.[43] As increasing the scan rate, the capacitive current density increased, indicating a good rate capability and lower internal resistances of the electrode materials. And the CV curves of coupled hybrid electrode retain a similar shape even up to the scan rate (160 mV s^{-1}), suggesting the good reversibility of the electrode materials in 1 M Na_2SO_4. For comparison the different scan rates (5-160 mV s^{-1}) CV curves of intermediate $CoSn(OH)_6$ and bare SnO_2 electrode are shown in Fig. S2 (a & b) are also rectangular in shape and exhibit mirror image characteristics which indicate that the electrochemical reactions are reversible as well as an ideal electrochemical capacitive behavior. However the current density of intermediate $CoSn(OH)_6$ and bare SnO_2 electrode material is lower than that of SnO_2-Co_3O_4 coupled hybrid. The higher current density of the coupled hybrid is due to the synergistic effect between the metal oxides in the electrode materials.

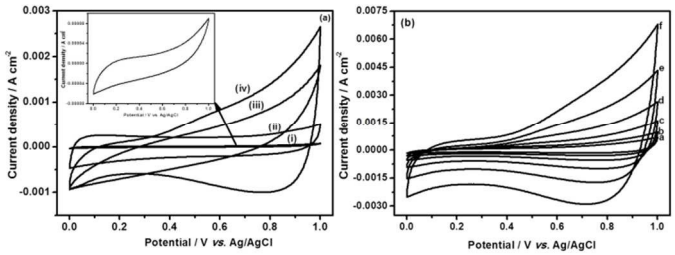

Fig. 6 CV curve for (a) bare SnO_2 (i), intermediate $CoSn(OH)_6$ (ii), pristine Co_3O_4 (iii) and SnO_2-Co_3O_4 coupled hybrid (iv) at 40 mV s^{-1} scan rate, (b) CV curve for SnO_2-Co_3O_4 coupled hybrid at different scan rates 5 mV s^{-1}, 10 mV s^{-1}, 20 mV s^{-1}, 40 mV s^{-1}, 80 mV s^{-1}, and 160 mV s^{-1} in the potential range between 0 to +1 V *vs*. Ag/AgCl in aqueous solution of 1 M Na_2SO_4 as electrolyte (a-f).

The galvanostatic charge-discharge behaviors of bare SnO_2, intermediate $CoSn(OH)_6$, pristine Co_3O_4 and SnO_2-Co_3O_4 coupled hybrid is investigated by chronopotentiometry from the potential range between 0 to +1 V *vs.* Ag/AgCl at the current density of 0.5 mA cm^{-2} in 1 M Na_2SO_4 electrolyte and it is shown in Fig. 7(a). A linear variation of potential vs. time is exhibited, which is another criterion for capacitive behavior of the electrode materials. This pseudocapacitance performance occurs from the electrochemical adsorption-desorption or redox reaction at an interface between the electrode and the electrolyte.[44] Evidently, the SnO_2-Co_3O_4 coupled hybrid possess considerably longer discharge time indicates that the higher capacitance of the SnO_2-Co_3O_4 coupled hybrid upon compared to that of bare SnO_2, intermediate $CoSn(OH)_6$ and pristine Co_3O_4. The specific capacitance can be calculated from the following formula

$$SC = It/m\Delta E \quad (1)$$

where, I is the charge – discharge current (A), t is the discharge time (s), m is the mass of the active material present on the electrode (g) and ΔE is the operating potential window (V) of charge or discharge. The calculated specific capacitance from the discharge curves (Fig. 7a) is 484 F g^{-1} for the SnO_2-Co_3O_4 coupled hybrid, which is much higher than that for the pristine Co_3O_4 (293 F g^{-1}), intermediate $CoSn(OH)_6$ (209 F g^{-1}) and bare SnO_2 (101 F g^{-1}) at the current density of 0.5 mA cm^{-2} in 1 M Na_2SO_4 electrolyte, respectively.

Approximately, the SnO_2-Co_3O_4 coupled hybrid is more than four fold larger than that for the bare SnO_2 and two fold larger than that for the pristine Co_3O_4, such enhanced capacitance of SnO_2-Co_3O_4 coupled hybrid is possibly assigned to the improved electrical conductivity and a high utilization of the electro active materials.

The obtained specific capacitance of our synthesized SnO_2-Co_3O_4 coupled hybrid was compared to other pristine Co_3O_4 and Sn–Co based mixed oxide. For example, porous Co_3O_4 materials prepared by solid-state thermolysis approach, exhibits a specific capacitance of 150 F g^{-1} at a current density of 1 A g^{-1} in 2 M KOH electrolyte[45]. Pang *et al.*[46] reported that dendrite-like Co_3O_4 nanostructure can deliver a specific capacitance of 207 F g^{-1} at a current density of 0.5 A g^{-1} in 3 M KOH electrolyte. Furthermore, mesoporous Co_3O_4 nanocubes were prepared by solid-state crystal re-construction route and displays a specific capacitance of 220 F g^{-1} at a current density of 0.6 A g^{-1} in 6 M KOH electrolyte[47]. Xie *et al.*[48] prepared layered Co_3O_4 material as a electrode material can deliver a specific capacitance 263 F g^{-1} at a current density of 1 A g^{-1} in 6 M KOH electrolyte. He *et al.*[49] prepared Sn-Co mixed oxide by co-precipitation method and reported supercapacitance of about 285 F g^{-1}. Ferreira *et al.*[50] also reported the supercapacitance of about 328 F g^{-1} for Ni-Co-Sn mixed oxide thin films prepared by Pechini method. The above results clearly indicate that our prepared SnO_2-Co_3O_4 coupled hybrid can deliver superior specific capacitance compared with these reported other cobalt oxide materials. The capacitance value reported in this work is much higher than these earlier reports, which is mainly assigned to the effective utilization of SnO_2 and Co_3O_4 materials and combined supercapacitive properties of both materials. Fig. 7 (b) shows the galvanostatic charge-discharge curves of SnO_2-Co_3O_4 coupled hybrid electrode at a current density of 0.5 mA cm^{-2}. For comparison the galvanostatic charge-discharge curves of intermediate $CoSn(OH)_6$ and bare SnO_2 electrode at a current density of 0.5 mA cm^{-2} are shown in Fig. S3 (a & b).

Cycling performance is another criterion in determining the applicability of supercapacitors for many practical applications. In this study, a long-term cycle stability of the SnO_2-Co_3O_4 coupled hybrid as an electrode material was evaluated by repeating the galvanostatic charge-discharge test at a current density of 0.5 mA cm^{-2} for 1000 cycles (Fig. 7(c)). During the first 100 cycles, the specific capacitance fades fast, decreasing by ~13% of its initial capacitance. During the next 600 cycles, the specific capacitance fades slightly and becomes stable, decreasing by ~5% of its initial capacitance. A considerable specific capacitance of 375 F g^{-1}, about 77% of initial capacitance is still retained after 1000 cycles indicates that good cycling stability and capacity retention of the coupled hybrid. The cycling performance and capacity retention in this work is higher compared to earlier report available in the literature.[45] For comparison a long-term cycle stability of the intermediate $CoSn(OH)_6$ and bare SnO_2 electrode was evaluated by repeating the galvanostatic charge-discharge test at a current density of 0.5 mA cm^{-2} for 1000 cycles (Fig. S4 (a & b)).

Rate capability is one of the key factors for evaluating the power applications of supercapacitors. Fig. 7(d) shows the galvanostatic charge-discharge curves of the supercapacitors electrode material made with SnO_2-Co_3O_4 coupled hybrid at different current densities (0.5 - 15 mA cm^{-2}) within the potential range between 0 to +1 V *vs.* Ag/AgCl. The specific capacitance values of the composite electrodes obtained from the discharge curves are 484, 472, 429, 400, 390, 386, 377, 371 and 343 F g^{-1} at the current density of 0.5, 1, 3 ,5 ,7, 9, 11, 13 and 15 mA cm^{-2}, respectively (Fig. 7 (e)). In general, the specific capacitance decreases with the increase in discharge current density, it may be caused by the increase of potential drop due to the resistance of the materials. In this cycling test, the charge-discharge time increases at lower current densities, ions from the electrolyte can diffuse into the inner-structure of electrode material, having access to almost all active sites of the electrode. Similarly, the charge-discharge time decreases at higher current densities, an effective utilization of the material is limited number of active sites to the outer surface of electrode. It reveals that the specific capacitance is inversely proportional to the current density.[51] When the current density increases from 0.5 to 15 mA cm^{-2} (484 F g^{-1} to 343 F g^{-1}), there is still around 71% of initial capacitance was retained, indicating the relatively excellent high-rate capability. These results confirmed that the coupled hybrid is ideally suitable for fast energy storage in supercapacitor applications.

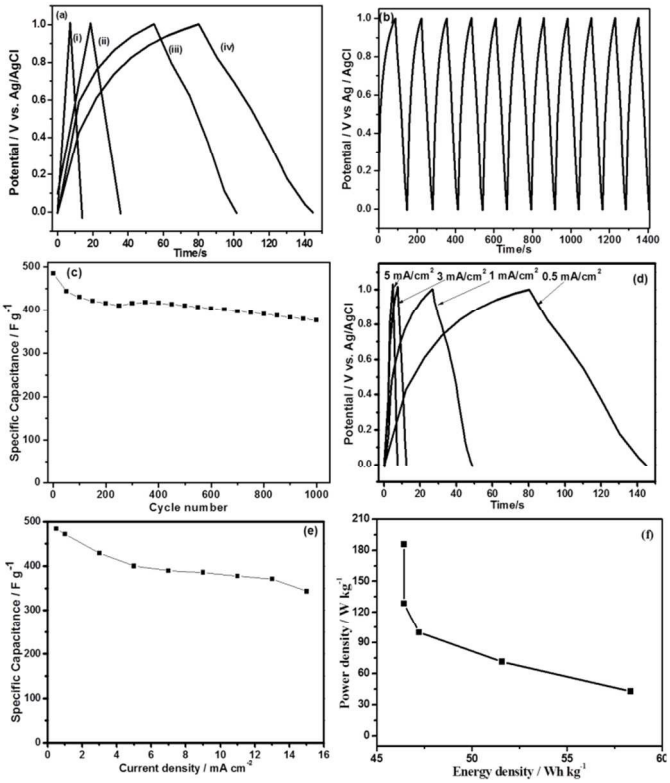

Fig. 7 (a) Charge–discharge cycles of bare SnO_2 (i), intermediate $CoSn(OH)_6$ (ii), pristine Co_3O_4 (iii) and SnO_2-Co_3O_4 coupled hybrid (iv) in aqueous solution of 1 M Na_2SO_4 at a current density of 0.5 mA cm^{-2} between 0 to +1 V *vs*. Ag/AgCl. Area of the electrode: 1.0 cm^2 (b) Charge–discharge cycles of SnO_2-Co_3O_4 coupled hybrid at a current density of 0.5 mA cm^{-2} (c) Cycling behavior of SnO_2-Co_3O_4 coupled hybrid (d) Galvanostatic charge discharge curves at different current densities 0.5 mA cm^{-2}, 1 mA cm^{-2}, 3 mA cm^{-2}, 5 mA cm^{-2} (e) Specific capacitance variation at different current densities (f) a Ragone plot for SnO_2-Co_3O_4 coupled hybrid.

The electrochemical parameters, such as energy and power density are an efficient way to evaluate the capacitive performance of supercapacitors. The energy density (E, W h kg^{-1}) and the power density (P, W kg^{-1}) for supercapacitors can be calculated using the following equations: [19]

$$E = (I*t*V) / (7.2*M) \text{ Wh/kg} \quad (2)$$

$$P = 3.6\ E / t \quad \text{W/kg} \quad (3)$$

where, E and P is the energy and power density respectively. I is the applied current (mA), t is the discharge time of the active material (s), V is the potential window (V) and M is the mass of the active material (mg). Fig. 7 (f) shows a Ragone plot for the SnO_2-Co_3O_4 coupled hybrid electrode. It is observed that energy density decreases with increasing power density. The energy density values are high, being 47– 67 W h kg^{-1}, while the power density values are in the range 215 – 100 W kg^{-1}.

The electrochemical impedance spectroscopy (EIS) can be applied for evaluating the kinetic and mechanistic information of electrode materials. The EIS are tested in the frequency range from 0.1–1,00,000 Hz at open circuit potential with amplitude of 10 mV, where Z' and Z'' are the real and imaginary parts of the impedance, respectively. Fig. 8 (a) shows the Nyquist plots of the EIS for bare SnO_2, intermediate $CoSn(OH)_6$, pristine Co_3O_4 and SnO_2-Co_3O_4 coupled hybrid. According to the analysis, the Nyquist plot of electrodes displays a semicircle in the high frequency region and a linear part in the low-frequency region. The diameter of semicircle presents in the high frequency region suggests that there is a charge transfer resistance (R_{ct}) in the electrochemical system, which is related with the diffusion of charge. Obviously, the smaller semicircle in SnO_2-Co_3O_4 coupled hybrid means charge transfer resistance (R_{ct}) decreased can be attributed due to the synergistic effect between the nanostructured metal oxides (SnO_2 and Co_3O_4), which may in turn responsible for improved electrical conductivity when compared to bare SnO_2, intermediate $CoSn(OH)_6$ and pristine Co_3O_4. This result indicates that the composite providing an ideal pathway for easy and fast penetration of the electrolyte ions into the inner layer of the coupled hybrid electrode. The vertical line at lower frequencies indicates an ideal capacitive behavior, representative of the ion diffusion of electrolyte within the pores of the electrode. Fig.8 (b) shows Nyquist plots of the EIS for SnO_2-Co_3O_4 coupled hybrid before and after 1000 cycles, the measured pseudo charge transfer resistance (R_{ct}) was increased, this further contributes to the decrease in specific capacitance after long term cyclic stability test.

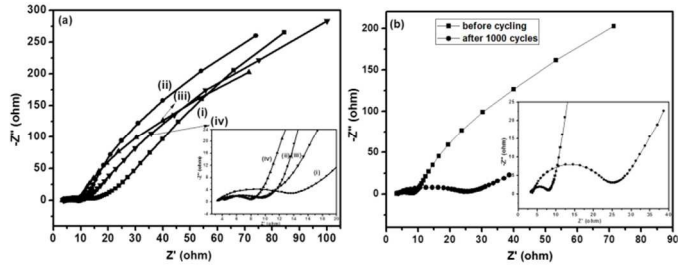

Fig. 8 Electrochemical impedance spectra of (a) bare SnO_2 (i), intermediate $CoSn(OH)_6$ (ii), pristine Co_3O_4 (iii) and SnO_2-Co_3O_4 coupled hybrid (iv), (b) SnO_2-Co_3O_4 coupled hybrid before and after 1000 cycles.

4. Conclusions

In summary, we have successfully synthesized cubic like nanostructured SnO_2-Co_3O_4 coupled hybrid via formation of intermediate $CoSn(OH)_6$ nanocubes. The XRD patterns indicate that the SnO_2-Co_3O_4 coupled hybrid with the tetragonal SnO_2 and cubic Co_3O_4 structure formed. The FE-SEM and HR-TEM images show that the coupled hybrid is still maintaining the original frame structure of $CoSn(OH)_6$ nanocubes. The electrochemical performance of the coupled hybrid electrode reaches a maximum specific capacitance upto 484 F g^{-1}, which is more than four-fold higher than that of bare SnO_2 (101 F g^{-1}) and it retains approximately 77% of initial specific capacitance after 1000 cycles, indicating good cycling stability of the composite. The excellent capacitive performance of the SnO_2-Co_3O_4 coupled hybrid is due to synergistic effect between the metal oxides and combined supercapacitive properties of both materials. These results suggest that these cubic like nanostructured SnO_2-Co_3O_4 coupled hybrid exhibit high specific capacitance, attractive rate capability may trust that it could be a potential candidate for supercapacitor application and in an energy storage technology in future.

Acknowledgements

The author SA and JJW thank DST, India (GITA/DST/TWN/P-50/2013) and NSC, Taiwan (NSC-101-2221-E-035-031-MY3) for the sanction of India–Taiwan collaborative research grant.

Notes and references

[*a] Nanomaterials and Solar Energy Conversion Lab, Department of Chemistry, National Institute of Technology, Trichy 620 015, India. E-mail : sanand@nitt.edu; Fax: +91-431-2300133 ; Tel: +91-431-2303639

[b] Department of Environmental Engineering and Science, Feng Chia University, Taichung 407, Taiwan

[c] The Center of Excellence for Advanced Materials Research, King Abdulaziz University, Jeddah 21413, P.O. Box 80203, Saudi Arabia.

1 D. V. Shinde, D. Y. Lee, S. A. Patil, I. Lim, S. S. Bhande, W. Lee, M. M. Sung, R. S. Mane, N. K. Shrestha and S. H. Han, *RSC Adv.,* 2013, **3**, 9431.

2 P. Simon and Y. GoGotSi, *Nat. Mater.,* 2008, **7,** 845.

3 S. Guo and S. Dong, *Chem. Soc. Rev.,* 2011, **40,** 2644.

4 S.P. Lim, N.M. Huang and H.N. Lim*, Ceram. Int.,* 2013, **39,** 6647.

5 Y. Yan, B. Wu, C. Zheng and D. Fang, *Mater. Sci. Appl.,* 2012, **3,** 377.

6 D. Cai, B. Liu, D. Wang, Y. Liu, L. Wang, H. Li, Y. Wang, C. Wang, Q. Li and T. Wang, *Electrochim. Acta,* 2014, **115,** 358.

7 E. Redondo, J. C. González, E. Goikolea, J. Ségalini and R. Mysyk, *Electrochim. Acta,* 2015, **160,** 178.

8 E. Frackowiak and F. Beguin, *Carbon,* 2001, **39,** 937.

9 H. R. Byon, S. W. Lee, S. Chen, P. T. Hammond and Y. Shao-Horn, *Carbon,* 2011, **49,** 457.

10 A. Devadas, S. Baranton, T. W. Napporn and C. Coutanceau*, J. Power Sources,* 2011, **196,** 4044.

11 B. Gnana Sundara Raj, A. M. Asiri, A. H. Qusti, J. J. Wu and S. Anandan, *Ultrason. Sonochem.,* 2014, **21,** 1933.

12 Q. Yang, Z. Lu, Z. Chang, W. Zhu, J. Sun, J. Liu, X. Sun and X. Duan, *RSC Adv.,* 2012, **2,** 1663.

13 T. Meng, P.P. Ma, J. L. Chang, Z. H. Wang and T. Z. Ren, *Electrochim. Acta,* 2014, **125,** 586.

14 X. Meng, M. Zhou, X. Li, J. Yao, F. Liu, H. He, P. Xiao and Y. Zhang, *Electrochim. Acta,* 2013, **109,** 20.

15 P. R. Deshmukh, S.N. Pusawale, V.S. Jamadade, U.M. Patil and C.D. Lokhande, *J. Alloys. Compd.,* 2011, **509,** 5064.
16 Y. Huang, J. Tao, W. Meng, M. Zhu, Y. Huang, Y. Fu, Y. Gao and C. Zhi, *Nano Energy,* 2015, **11,** 518.
17 G. A. Snook, P. Kao and A. S. Best, *J. Power Sources,* 2011 **196,** 1.
18 J. Zhang, D. Shu, T. Zhang, H. Chen, H. Zhao, Y. Wang, Z. Sun, S. Tang, X. Fang and X. Cao, *J. Alloys. Compd.,* 2012, **532,** 1.
19 B. Gnana Sundara Raj, R. R. Ramprasad, A. M. Asiri, J. J. Wu and S. Anandan, *Electrochim. Acta,* 2015, **156,** 127.
20 Z. Luo, Y. Zhu, E. Liu, T. Hu, Z. Li, T. Liu and L. Song, *Mater. Res. Bull.* 2014, **60,** 105.
21 B. Gnana Sundara Raj, A. M. Asiri, J. J. Wu and S. Anandan, *J. Alloys. Compd.,* 2015, **636,** 234.
22 S.N. Pusawale, P.R. Deshmukh, J.L. Gunjakar and C.D. Lokhande, *Mater. Chem. Phys.,* 2013, **139,** 416.
23 J. S. Chen, M. F. Ng, H. B. Wu, L. Zhang and X. W. (David) Lou, *Cryst. Eng. Comm.,* 2012, **14,** 5133.
24 C. Ma, J. Lu, W. Shao, F. Gu and S. Jing, *Int. J. Electrochem. Sci.,* 2013, **8,** 3580.
25 C. Karunakaran, S. Sakthi Raadha and P. Gomathisankar, *J. Alloys. Compd.,* 2013, **549,** 269.
26 Y. Kuang, G. Chen, X. Lei, L. Luo and X. Sun, *Sensor. Actuat. B - Chem.,* 2013, **181,** 629.
27 H. Xu, J. Zhuang, Y. Chen, J. Wu and J. Zhang, *RSC Adv.,* 2014, **4,** 15511.
28 J. Liu, J. Jiang, M. Bosman and H. J. Fan, *J. Mater. Chem.,* 2012, **22,** 2419.
29 H. Jiang, C. Li, T. Sun and J. Ma, *Chem. Commun.,* 2012, **48,** 2606.
30 J. H. Zhong, A. L. Wang, G. R. Li, J. W. Wang, Y. N. Ou and Y. X. Tong, *J. Mater. Chem.,* 2012, **22,** 5656.
31 R. Li, X. Ren, F. Zhang, C. Du and J. Liu, *Chem. Commun.,* 2012, **48,** 5010.
32 M. Jayalakshmi, M. Mohan Rao, N. Venugopal and K. B. Kim, *J. Power Sources,* 2007, **166,** 578.
33 A. M. Hashem, H. M. Abuzeid, A.E. Abdel-Ghany, A. Mauger, K. Zaghib and C.M. Julien, *J. Power Sources,* 2012, **202,** 291.
34 V.R. Shinde, S.B. Mahadik, T.P. Gujar and C.D. Lokhande, *Appl. Surf. Sci.,* 2006, **252,** 7487.
35 K. Karthikeyan, S. Amaresh, D. Kalpana, R. Kalai Selvan and Y.S. Lee, *J. Phys. Chem. Solids,* 2012, **73,** 363.
36 S. Ibarra-Trevino, L. L. Garza-Tovar, E. Sanchez and L. C. Torres-Gonzalez*, J. Mater. Sci-Mater. El.,* 2013, **24,** 3219.
37 S. Das, S. Chaudhuri, and S. Maji, *J. Phys. Chem. C,* 2008, **112,** 6213.
38 V. S. R. Channu, R. Holze, S. A. Wicker Sr., E. H. Walker Jr., Q. L. Williams and R. R. Kalluru, *Mater. Sci. Appl.,* 2011, **2,** 1175.
39 H. Jena, K.V. Govindan Kutty and T.R.N. Kutty, *Mater. Chem. Phys.,* 2004, **88,** 167.
40 F. Huang, Z. Yuan, H. Zhan, Y. Zhou and J. Sun, *Mater. Chem. Phys.,* 2004, **83,** 16.
41 M. M. Rahman, S. B. Khan, M. Faisal, M. A. Rub, A. O. Al-Youbi and A. M. Asiri, *Talanta,* 2012, **99,** 924.
42 Y. Gao, S. Chen, D. Cao, G. Wang and J. Yin, *J. Power Sources*, 2010, **195,** 1757.
43 F. Zhang, X. G. Zhang and L. Hao, *Mater. Chem. Phys.,* 2011, **126,** 853.
44 F. Tao, Y. Q. Zhao, G. Q. Zhang and H. L. Li, *Electrochem. Commun.,* 2007, **9,** 1282.
45 F. Meng, Z. Fang, Z. Li, W. Xu, M. Wang, Y. Liu, J. Zhang, W. Wang, D. Zhao and X. Guo, *J. Mater. Chem.* A, 2013, **1,** 7235.
46 H. Pang, F. Gao, Q. Chen, R. Liu and Q. Lu, *Dalton Trans.,* 2012, **41 ,** 5862.
47 X. Liu, Q. Long, C. Jiang, B. Zhan, C. Li, S. Liu, Q. Zhao, W. Huang and X. Dong, *Nanoscale,* 2013, **5,** 6525.
48 L. Xie, K. Li, G. Sun, Z. Hu, C. Lv, J. Wang and C. Zhang, *J. Solid State Electrochem.,* 2013, **17,** 55.
49 P. He, Z. Xie, Y. Chen, F. Dong and H. Liu, *Mater. Chem. Phys.,* 2012, **137,** 576.
50 C. S. Ferreira, R. R. Passos and L. A. Pocrifka, *J. Power Sources*, 2014, **271,** 104.
51 Y. Liu, W. Wang, Y. Wang, Y. Ying, L. Sun and X. Peng, *RSC Adv.,* 2014, **4,** 16374.

Hybrid SnO_2-Co_3O_4 nanocubes prepared via $CoSn(OH)_6$ intermediate through sonochemical route for Energy Storage Applications

Balasubramaniam Gnana Sundara Raj[a], Jerry J Wu[b], Abdullah M. Asiri[c], Sambandam Anandan[a,*]

[a]Nanomaterials and Solar Energy Conversion Lab, Department of Chemistry, National Institute of Technology, Trichy 620 015, India.
[b]Department of Environmental Engineering and Science, Feng Chia University, Taichung 407, Taiwan.
[c]The Center of Excellence for Advanced Materials Research, King Abdulaziz University, Jeddah 21413, P.O. Box 80203, Saudi Arabia.

[*]To whom correspondence should be addressed: E-mail: sanand@nitt.edu; sanand99@yahoo.com; Tel.: +91-431-2503639; Fax: +91 431 2500133.

Graphical abstract